Contribution from the Department of Chemistry,
Emory University, Atlanta, Georgia 30322

Structural and Electronic Properties of Six-Coordinate Manganese(III) Porphyrin Cations. Crystal and Molecular Structure of Bis(*N*,*N*-dimethylformamide)(tetraphenylporphinato)manganese(III) Perchlorate, $[Mn^{III}TPP(DMF)_2]^+ClO_4^-$

CRAIG L. HILL* and MICHAEL M. WILLIAMSON

Received September 24, 1984

In toluene or chloride-free chloroform solutions of $Mn^{III}TPP(ClO_4)$ in the presence of the neutral ligands L = dimethylformamide, dimethylacetamide, 1-methylimidazole, dimethyl sulfoxide, and tetrahydrofuran the six-coordinate cationic complexes $[Mn^{III}TPP(L)_2]^+ClO_4^-$ form. One of these complexes, bis(*N*,*N*-dimethylformamide)(tetraphenylporphinato)manganese(III) perchlorate, $[Mn^{III}TPP(DMF)_2]^+ClO_4^-$ (**1**), was isolated, purified, and characterized in detail. The electronic spectra, ^1H NMR spectra, and magnetic properties of **1** in solution establish that this complex contains a high-spin $S = 2$ Mn^{III} atom with a $(d_{xz}\pi, d_{yz}\pi)^2(d_{xy})^1(d_{z^2}\sigma)^1$ electronic configuration. The variable-temperature ^1H NMR data furthermore rule out any change in ground electronic state over the temperature range −30 to +55 °C. All the cationic Mn^{III} porphyrin complexes undergo fast exchange of the neutral axial ligands, L, on the NMR time scale even at −40 °C. Complex **1** forms solvate-free crystals in space group $C2/c$. The unit cell has $a = 17.7386$ (43) Å, $b = 17.7182$ (60) Å, $c = 15.9477$ (56) Å, $\beta = 118.693$ (22)°, and $Z = 4$. The structure was solved by the heavy-atom method and converged with a final $R = 0.0841$. The six-coordinate $S = 2$ Mn^{III} atom displays the predicted tetragonal elongation with very long Mn^{III}–O(DMF) bonds (2.217 (4) Å). Complex **1** shows a temperature-dependent alteration of coordination geometry in solution with the six-coordinate species predominating below −10 °C and a five-coordinate species predominating above +10 °C.

Introduction

Manganese porphyrins have successfully been used as catalysts for the mild homogeneous oxidation of several organic functions, including hydrocarbons.[1,2] Some Mn porphyrin based systems display the richest homogeneous catalytic alkane functionalization chemistry to date.[1] It also was recently demonstrated that water-soluble Mn porphyrins are capable of oxidizing water to either H_2O_2 or O_2 in thermal and photochemical processes.[3] All this recent oxidation chemistry has provided impetus for the purification and characterization of Mn^{IV} [4-10] and Mn^V porphyrin[11,12] complexes much as earlier work using Mn porphyrins as heme models provided impetus for the purification and characterization of Mn^{II} [13-15] and Mn^{III} [16-20] porphyrin complexes.

Under ambient laboratory conditions and in the presence of air the divalent oxidation state is the most stable one for Mn in a great majority of Mn coordination compounds. In constrast, the trivalent state is almost always the most stable state for Mn in porphyrins.[13,21] The d^4 Mn^{III} ion in Mn porphyrins is nearly always in the high-spin $S = 2$ state although Reed, Scheidt, and co-workers demonstrated that low-spin $S = 1$ Mn^{III} porphyrin complexes form if imidazolate ligands occupy both axial positions.[20] More recently, Hansen and Goff demonstrated that two axially coordinated cyanide ligands also produce a low-spin Mn^{III} porphyrin complex.[22] The predominant forms of the conventional high-spin $S = 2$ Mn^{III} porphyrin complexes in solution have been thought to be one of the two forms that have been characterized by X-ray crystallography, the five-coordinate species, $Mn^{III}(Por)X$, or the six-coordinate species, $Mn^{III}(Por)(L)X$, when L = a neutral ligand and X = an anionic ligand, despite the fact that there has been evidence for the presence of other Mn^{III} porphyrin species in solution dating back to the early work of Boucher.[21] We have undertaken an investigation of a third coordination form of $[Mn^{III}(Por)]^+$ that exists in solution, the six-coordinate Mn^{III} porphyrin cations $[Mn^{III}(Por)(L)_2]^+X^-$. Since the electronic and structural properties of these species are likely of direct relevance to recently investigated catalytic and redox processes of Mn porphyrins,[1,2] we have prepared, isolated, and characterized the ground-state electronic properties of some Mn^{III} porphyrin cations, $[Mn^{III}TPP(L)_2]^+X^-$, and examined one exemplary complex, bis(*N*,*N*-dimethylformamide)(tetraphenylporphinato)manganese(III) perchlorate, $[Mn^{III}TPP(DMF)_2]^+ClO_4^-$ (**1**), in detail including its X-ray crystal structure.[23] Hoard and co-workers

(1) (a) Schardt, B. C.; Hill, C. L. *J. Am. Chem. Soc.* **1980**, *102*, 6374. (b) Hill, C. L.; Smegal, J. A. *Nouv. J. Chim.* **1982**, *6*, 287. (c) Smegal, J. A.; Hill, C. L. *J. Am. Chem. Soc.* **1983**, *105*, 3515. (d) Smegal, J. A.; Hill, C. L. *J. Am. Chem. Soc.* **1983**, *105*, 2920. (e) Hill, C. L.; Smegal, J. A.; Henly, T. J. *J. Org. Chem.* **1983**, *48*, 3277.
(2) (a) Tabushi, I.; Koga, N. *J. Am. Chem. Soc.* **1979**, *101*, 6456. (b) Tabushi, I.; Koga, N. *Tetrahedron Lett.* **1979**, 3681. (c) Groves, J. T.; Kruper, W. J., Jr.; Haushalter, R. C. *J. Am. Chem. Soc.* **1980**, *102*, 6375; **1981** *103*, 778. (d) Guilmet, E.; Meunier, B. *Tetrahedron Lett.* **1980**, 4449. (e) Mansuy, D.; Bartoli, J.-F.; Chottard, J.-C.; Lange, M. *Angew. Chem., Int. Ed. Engl.* **1980**, *19*, 909. (f) Chang, C. K.; Ebina, F. *J. Chem. Soc., Chem. Commun.* **1981**, 778. (g) Perrée-Fauvet, M.; Gaudemer, A. *J. Chem. Soc., Chem. Commun.* **1981**, 874. (h) Tabushi, I.; Yazaki, A. *J. Am. Chem. Soc.* **1981**, *103*, 7371. (i) Guilmet, E.; Meunier, B. *Nouv. J. Chim.* **1982**, *6*, 511. (j) Groves, J. T.; Takahashi, T. *J. Am. Chem. Soc.* **1983**, *105*, 2073. (k) Groves, J. T.; Watanabe, Y.; McMurry, T. J. *J. Am. Chem. Soc.* **1983**, *105*, 4489. (l) Collman, J. P.; Kodadek, T.; Raybuck, S. A.; Meunier, B. *Proc. Natl. Acad. Sci. U.S.A.* **1983**, *80*, 7039. (m) Collman, J. P.; Brauman, J. I.; Meunier, B.; Raybuck, S. A.; Kodadek, T. *Proc. Natl. Acad. Sci. U.S.A* **1984**, *81*, 3245.
(3) (a) Harriman, A.; Porter, G. *J. Chem. Soc., Faraday Trans. 2* **1979**, *75*, 1543. (b) Porter, G. *Proc. R. Soc. London, Ser. A* **1978**, *362*, 281. (c) Tabushi, I.; Kojo, S. *Tetrahedron Lett.* **1975**, 305.
(4) Schardt, B. C.; Hollander, F. J.; Hill, C. L. *J. Am. Chem. Soc.* **1982**, *104*, 3964.
(5) Camenzind, M. J.; Hollander, F. J.; Hill, C. L. *Inorg. Chem.* **1982**, *21*, 4301.
(6) Smegal, J. A.; Schardt, B. C.; Hill, C. L. *J. Am. Chem. Soc.* **1983**, *105*, 3510.
(7) Smegal, J. A.; Hill, C. L. *J. Am. Chem. Soc.* **1983**, *105*, 2920.
(8) Camenzind, M. J.; Hollander, F. J.; Hill, C. L. *Inorg. Chem.* **1983**, *22*, 3776.
(9) (a) Camenzind, M. J.; Hill, C. L. *Inorg. Chem.* **1984**, *23*, 1984. (b) Birchall, T. J.; Smegal, J. A.; Hill, C. L. *Inorg. Chem.* **1984**, *23*, 1910.
(10) Bortolini, O.; Meunier, B. *J. Chem. Soc., Chem. Commun.* **1983**, 1364.
(11) Hill, C. L.; Hollander, F. J. *J. Am. Chem. Soc.* **1982**, *104*, 7318.
(12) (a) Buchler, J. W.; Dreher, C.; Lay, K. L. *Z. Naturforsch., B: Anorg. Chem., Org. Chem.* **1982**, *37B*, 1155. (b) Buchler, J. W.; Dreher, C.; Lay, K. L.; Lee, Y. J. A.; Scheidt, W. R. *Inorg. Chem.* **1983**, *22*, 888.
(13) Gonzalez, B.; Kouba, J.; Yee, S.; Reed, C. A.; Kirner, J. F.; Scheidt, W. R. *J. Am. Chem. Soc.* **1975**, *97*, 3247.
(14) Kirner, J. F.; Reed, C. A.; Scheidt, W. R. *J. Am. Chem. Soc.* **1977**, *99*, 1093.
(15) Kirner, J. F.; Reed, C. A.; Scheidt, W. R. *J. Am. Chem. Soc.* **1977**, *99*, 2557.
(16) Day, V. W.; Stults, B. R.; Tasset, E. L.; Marianelli, R. S.; Boucher, L. J. *Inorg. Nucl. Chem. Lett.* **1975**, *11*, 505.
(17) Day, V. W.; Stults, B. R.; Tasset, E. L.; Day, R. O.; Marianelli, R. S. *J. Am. Chem. Soc.* **1974**, *96*, 2650.
(18) Kirner, J. F.; Scheidt, W. R. *Inorg. Chem.* **1975**, *14*, 2081.
(19) Tulinsky, A.; Chen, B. M. L. *J. Am. Chem. Soc.* **1977**, *99*, 3647.
(20) Landrum, J. T.; Hatano, K.; Scheidt, W. R.; Reed, C. A. *J. Am. Chem. Soc.* **1980**, *102*, 6729.
(21) Boucher, L. J. *Coord. Chem. Rev.* **1972**, *7*, 289.
(22) Hansen, A. P.; Goff, H. M. *Inorg. Chem.* **1984**, *23*, 4519.
(23) Abbreviations: TPP = dianion of 5,10,15,20-tetraphenylporphyrin; DMF = *N*,*N*-dimethylformamide; DMA = *N*,*N*-dimethylacetamide; Me_2SO = dimethyl sulfoxide; THF = tetrahydrofuran; 1-MeIm = 1-methylimidazole; Pc = phthalocyanine.

0020-1669/85/1324-2836$01.50/0

Table I. Crystal and Data Collection Parameters for $[Mn^{III}TPP(DMF)_2]^+ClO_4^-$ (**1**)

(A) Crystal Parameters at 25 °C[a,b]

space group: $C2/c$ (No. 15, C_{2h}^6)	V = 4396.8 (25) Å^3
Z = 4	M_r = 913.3
a = 17.7386 (43) Å	d_{calcd} = 1.38 g cm^{-3}
b = 17.7182 (60) Å	d_{obsd} = 1.36 (2) g cm^{-3}
c = 15.9477 (56) Å	μ_{calcd} = 4.04 cm^{-1}
β = 118.693 (22)°	cryst dimens: 0.56 × 0.16 × 0.18 mm

(B) Data Measurement

radiation: Mo K$\bar{\alpha}$ (λ = 0.71069 Å)
monochromator: highly oriented graphite ($2\theta_M$ = 12.2°)
perpendicular mode, assumed 50% perfect
reflcns measd: $\pm h,+k,+l$
2θ range: 4.6–50°
scan type: θ–2θ
scan speed (θ): 2.02 (min), 29.3 (max) deg/min
bkgd/scan time = 1
reflcns collected: 4311
unique reflcns used in least squares: 2671 with $F_o > 2.5\sigma F_o$
std reflcns: 0,0,6; 0,8,0; 8,0,0; measd every 97 reflcns

[a] Unit cell parameters were derived by a least-squares fit of 15 centered reflections with 2θ between 13.02 and 23.13°. [b] In this and all subsequent tables the esd's of all parameters are given in parentheses of the least significant digit(s) given.

reported the crystallographic characterization of a bis(1-methylimidazole) Mn^{III} porphyrin complex.[24]

Experimental Section

Physical Measurements. Elemental analyses were performed by Atlantic Microlab, Inc. Infrared spectra of samples 2 wt % in KBr were obtained with a Perkin-Elmer Model 1430 infrared spectrophotometer. The samples were pulverized with KBr in a "Wig-L-Bug" apparatus by shaking for brief (ca. 10 s) intervals to avoid decomposition of the $[Mn^{III}TPP(L)_2]^+ClO_4^-$ species. *Caution! Although* **1** *and the other cationic complexes reported here have given no indication of sensitivity to shock or grinding, perchlorate salts such as these are potentially dangerous and related materials have been known to detonate.* The electronic spectra (325–700 nm) were recorded on a Hewlett-Packard (H/P) Model 8451A multidiode array UV–vis spectrometer. Magnetic susceptibilities were determined by the Evans method.[25] Variable-temperature and other ^1H NMR spectra were obtained with a Nicolet Model 360-NB 360-MHz spectrometer. The crystallography is described below.

Materials. All solvents and chemicals were of reagent or analytical grade. Toluene was purified before use by successive treatment with concentrated H_2SO_4, H_2O, NaOH (aq), and H_2O dried with anhydrous $MgSO_4$, and then fractionally distilled from P_2O_5. *N,N*-Dimethylformamide, glass-distilled grade from Burdick and Jackson, was used without further purification. Toluene-d_8 and $CDCl_3$ for NMR studies were both "100.0 atom % D" grade purchased from Aldrich. The complexes $Mn^{III}TPP(OAc)$ and $Mn^{III}TPP(Cl)$ were prepared by literature methods,[6] and $Mn^{III}TPP(ClO_4)$ was prepared by metathesis of $Mn^{III}TPP(Cl)$ with 1.05 equiv of $AgClO_4$ in hot toluene and recrystallized from hot toluene/heptane.

Synthesis of Bis(*N*,*N*-dimethylformamide)(tetraphenylporphinato)manganese(III) Perchlorate (1). $Mn^{III}TPP(ClO_4)$ (100 mg, 0.13 mmol) was dissolved in 25 mL of highly purified dimethylformamide (DMF). To the stirred DMF solution was added triple-distilled water dropwise until the first cloudiness became persistent. The sample was allowed to stand overnight, during which time very dark red-purple crystals formed. The crystals were collected and dried in vacuo to produce a 90% yield of **1**. Anal. Calcd for $C_{50}H_{42}ClMnN_6O_6$ (solvate-free $[MnTPP(DMF)_2]^+ClO_4^-$): C, 65.75; H, 4.64; N, 9.20. Found: C, 65.71; H, 4.68; N, 9.12. The spectroscopic properties of this reactive complex are described in the Results and Discussion.

X-ray Crystallography. Collection and Reduction of Intensity Data. One representative deep red-purple crystal was attached to the end of a glass fiber with epoxy cement, and then the fiber was mounted on a goniometer head of a Syntex $P2_1$ four-circle diffractometer equipped with a graphite monochromator and scintillation counter with pulse height discrimination. After the crystal was centered, accurate cell dimensions were determined by least-squares refinement of 15 centered reflections (2θ = 13.05–23.13°; λ(Mo Kα) = 0.71069 Å). The θ–2θ scan method with a variable scan rate of 2.02–29.3°/min (scan time/background = 1) was used. Intensity measurements of 3 standards every 97 reflections showed no evidence of crystal deterioration. Intensities (2θ = 4.59–50.0°) were measured for 3893 reflections, of which 2677 unique reflections were observed ($F \geq 2.5\sigma(F)$). The crystal and data collection parameters are summarized in Table I.

Table II. Atom Coordinates (×10^4) and Temperature Factors (10^3 Å^2)

atom	x	y	z	U[a]
Mn	0	0	0	36 (1)
O(1a)	589 (3)	508 (3)	1448 (3)	76 (2)
N(1)	1106 (3)	−534 (2)	353 (3)	38 (2)
N(2)	421 (3)	889 (2)	−450 (3)	39 (2)
C(1)	1807 (3)	−275 (3)	258 (3)	38 (2)
C(2)	2468 (3)	−842 (3)	609 (4)	45 (3)
C(3)	2178 (3)	−1432 (3)	907 (4)	45 (3)
C(4)	1336 (3)	−1253 (3)	746 (3)	37 (2)
C(5)	825 (3)	−1740 (3)	937 (4)	38 (2)
C(6)	−2 (3)	1568 (3)	−782 (4)	39 (3)
C(7)	562 (4)	2077 (3)	−909 (4)	54 (3)
C(8)	1292 (4)	1721 (3)	−685 (4)	51 (3)
C(9)	1219 (3)	971 (3)	−403 (4)	40 (3)
C(10)	1860 (3)	422 (3)	−113 (4)	40 (2)
C(11)	2625 (3)	586 (3)	−244 (4)	41 (3)
C(12)	3452 (4)	581 (3)	510 (4)	52 (3)
C(13)	4147 (4)	732 (4)	374 (5)	59 (3)
C(14)	4023 (4)	874 (3)	−540 (5)	63 (3)
C(15)	3208 (4)	880 (3)	−1296 (4)	51 (3)
C(16)	2515 (3)	737 (3)	−1144 (4)	48 (3)
C(17)	1176 (3)	−2502 (3)	1339 (4)	37 (2)
C(18)	1496 (5)	−2637 (3)	2296 (4)	76 (4)
C(19)	1827 (5)	−3342 (4)	2680 (5)	90 (4)
C(20)	1805 (4)	−3915 (4)	2112 (5)	69 (4)
C(21)	1480 (4)	−3789 (3)	1163 (5)	57 (3)
C(22)	1165 (4)	−3082 (3)	768 (4)	49 (3)
C(2a)	840 (4)	786 (4)	2276 (6)	101 (5)
N(3a)	1001 (3)	1512 (3)	2449 (3)	57 (2)
C(4a)	1260 (5)	1757 (6)	3403 (5)	123 (5)
C(5a)	995 (6)	2069 (6)	1818 (7)	146 (7)
Cl	5000	−956 (1)	2500	58 (1)
O(2)	4405 (4)	−487 (4)	2579 (4)	139 (4)
O(3)	5427 (4)	−1381 (3)	3353 (4)	118 (3)

[a] Equivalent isotropic U defined as one-third of the trace of the orthogonalized **U** tensor.

Structure Solution and Refinement. The structure was solved by using a Data General Eclipse S-140 computer with Nicolet SHELXTL software. The data exhibited the systematic absences hkl ($h + k = 2n + 1$) and $h0l$ ($l = 2n + 1$) and thus suggest Cc or $C2/c$ as the only likely space groups. The statistical distribution of normalized structure factors, E, strongly indicates a centric space group ($||E|^2 - 1|_{av} = 0.96$). The structure was solved in the only centric space group of the two choices, $C2/c$. The position of the Mn atom, located by conventional Patterson synthesis, lay on the inversion center 0, 0, 0; the Cl atom lay on a 2-fold axis. All non-hydrogen atoms were located in subsequent difference Fourier synthesis. Non methyl hydrogen atoms were initially placed in their calculated positions and then were allowed to refine independently. The methyl hydrogens of the DMF were allowed to "ride" on their parent carbon (C–H = 0.96 Å; $U_{iso}(H) = 1.2[U_{ij}(C)]$). The final electron density map was clean, except for a positive peak (1.1 e Å^{-3}) 1.26 Å from O1a of the DMF ligand; all other peaks were <0.6 e Å^{-3}. Block-cascade matrix least-squares refinement of 347 variables gave final agreement factors of R = 0.0841 and R_w = 0.0761, where $R = \sum||F_o| - |F_c||/|F_o|$ and $R_w = [\sum w(|F_o| - |F_c|)^2/w|F_o|^2]^{1/2}$. The GOF value was 1.567; GOF = $(\sum w(|F_o| - |F_c|)^2/n_o - n_v)^{1/2}$. On the last cycle of the least-squares refinement the ratio of maximum shift to the estimated standard deviation was −0.021. The data were corrected for Lorentz–polarization, and no absorption correction was performed. A weighting scheme, utilizing weights of the form $w = [\sigma^2(F_o) + |g|F_o^2]^{-1}$ (where g = 0.00086), was implemented as a result of an analysis of the data set as a function of F_o, 2θ, and hkl. Scattering factors were those for neutral atoms;[26] final

(24) Steffen, W. L.; Chun, H. K.; Hoard, J. L. "Abstracts of Papers", 175th National Meeting of the American Chemical Society, Anaheim, CA, March 1978; American Chemical Society: Washington, DC, 1978; INOR 15.
(25) Evans, D. F. *J. Chem. Soc.* **1959**, 2003.
(26) Cromer, D. T.; Waber, J. T. "International Tables for X-ray Crystallography"; Kynoch Press: Birmingham, England, 1974; Vol. IV, Table 2.2B.

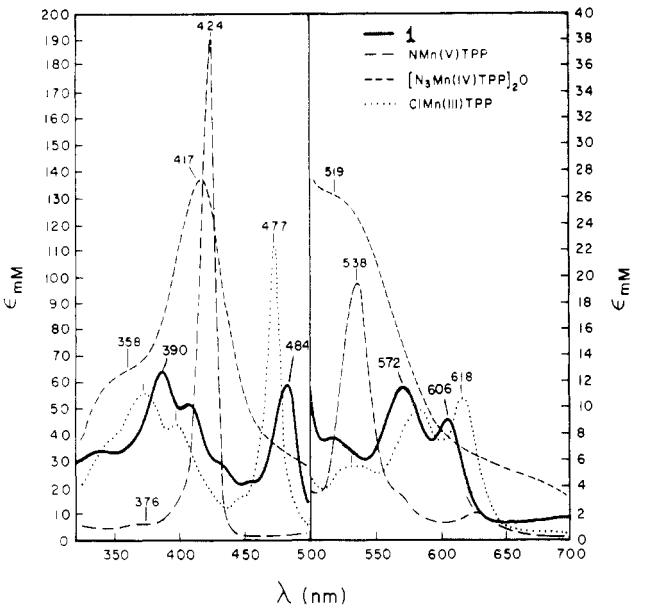

Figure 1. Electronic spectra of a six-coordinate Mn^{III} porphyrin cation, **1**, compared with the electronic spectra of representative Mn^{IV}, Mn^{V}, and five-coordinate Mn^{III} porphyrin complexes: (—) **1**; (--) $NMn^{V}TPP$; (---) $[N_3Mn^{IV}TPP]_2O$; (···) $ClMn^{III}TPP$. The spectrum of $NMn^{V}TPP$ for λ = 325–500 nm is half-scale. All spectra are recorded as ca. 1 mM solutions in toluene at 25 °C.

positional and thermal parameters are given in Table II.

Selected bond lengths and angles are given in Tables III and IV in the Results and Discussion. Anisotropic temperature factors (Table SVI), hydrogen atom coordinates and isotropic temperature factors (Table SVII), and observed and calculated structure factors (Table SVIII) are available as supplementary material.

Results and Discussion

Syntheses and Stability of Cationic Six-Coordinate Mn^{III} Porphyrin Complexes. The six-coordinate cations, $[Mn^{III}(Por)L_2]^+X^-$, are the predominant species in solution when a Mn^{III} porphyrin complex such as $Mn^{III}TPP(X)$ containing a weakly coordinating or noncoordinating anionic ligand, X, is treated with ≥2 equiv of reasonably strong neutral ligand, L. The $[Mn^{III}TPP(L)_2]^+ClO_4^-$ complexes can be isolated by addition of heptane to a solution of $Mn^{III}TPP(ClO_4)$ in toluene containing L or by addition of water to a solution of $MnTPP(ClO_4)$ in L, when L = DMF, 1-methylimidazole, DMA, Me_2SO, and THF.[23] The affinity of the high-spin $S = 2$ Mn^{III} ion in porphyrin complexes for halide and pseudohalide ligands is so high that dissolving the above complexes in any but the most highly purified chlorocarbon solvents ($CHCl_3$ and CH_2Cl_2) results in the immediate and quantitative production of the $Mn^{III}TPP(Cl)$ complex.

Electronic and Magnetic Properties. The electronic spectra (325–700 nm) of **1** compared with the spectra of representative Mn^{III}, Mn^{IV}, and Mn^{V} porphyrin complexes we have previously characterized are illustrated in Figure 1.[4-9,11] Complex **1** displays a d-type hyperporphyrin spectrum typical of high-spin Mn^{III} porphyrin complexes.[27] All show distinct split Soret bands and several extra bands in the visible region. This spectrum is distinct from those of Mn^{II}, Mn^{IV}, and Mn^{V} porphyrin complexes and similar yet still distinct from the few electronic spectra available on low-spin $S = 1$ Mn^{III} porphyrin complexes.[22] The magnetic moment of **1** determined by the Evans method is the same within experimental error as that for $Mn^{III}TPP(Cl)$, or 4.9 μ_B.[25,28] This is the theoretically predicted magnetic moment for a D_{4h} high-spin d^4 complex displaying minimal spin–orbit coupling.

Infrared Spectra of 1. Infrared spectra of **1** and related six-coordinate Mn^{III} porphyrin cations can be obtained in the solid state as KBr pellets if care is taken to avoid heating during the pellet preparation process. If the KBr and the complex are individually prepulverized and then shaken together for less than 10 s prior to pressing, the complex is not decomposed. If the KBr and the complex are shaken together longer than 20 s, a smooth decomposition in the solid state begins to take place in which a DMF molecule is displaced from an axial position of the Mn^{III} atom, forming the more stable $Mn^{III}TPP(Br)(L)$ complex. The displaced free DMF is readily distinguished from the DMF ligated to Mn by IR spectroscopy (Figure 2). The DMF carbonyl stretching frequency shifts from 1658 cm^{-1} in **1** to ca. 1675 cm^{-1} in the decomposed sample. The value for free DMF is 1675 cm^{-1}.[29] The intensity of the DMF carbonyl stretch is much higher when DMF is complexed to Mn than when it is free. The frequencies and intensities of the DMF methyl C–H stretching fundamentals at ca. 2872 and 2935 cm^{-1} are minimally perturbed upon complexation to a metal, as expected. The ratio of the intensity of the C=O stretch to the intensity of the methyl C—H stretch (2935 cm^{-1}) goes from ca. 3 in free DMF to ca. 15 in **1**. Similar carbonyl stretching frequency shifts and intensity changes have been observed upon complexation of DMF[29] and peptide amides to d^0 metal ions.[30] In all these cases the DMF is ligating to the metal by the lone pairs on the oxygen atom and the metal–oxygen interaction is primarily electrostatic in nature. These effects can be rationalized qualitatively by the equilibrium in eq 1 or by the

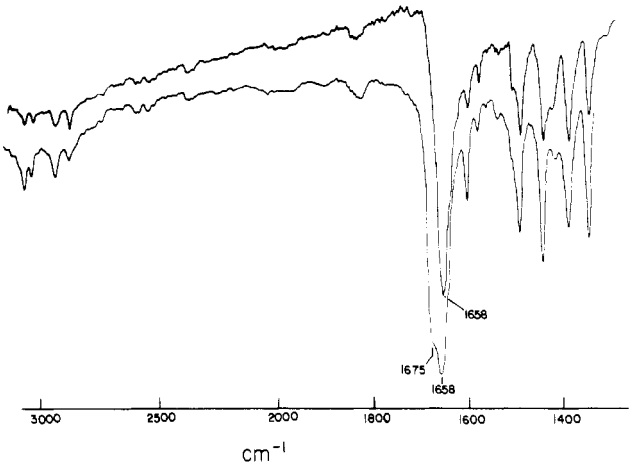

Figure 2. Infrared spectra of **1** in KBr before decomposition (top) and after decomposition (>20 s shaking in "Wig-L-Bug" apparatus at 25 °C) to $Mn^{III}TPP(Br)(DMF)$ + free DMF (bottom). The poor base line in the top spectrum is a consequence of the large particle size resulting from limited shaking times (≤10 s).

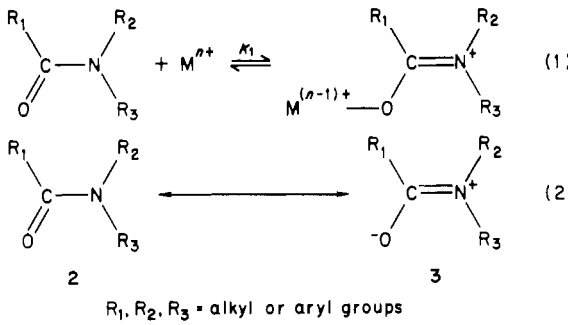

fact that ligation to the metal perturbs the amide molecule such that the zwitterionic canonical form, **3**, becomes more highly favored (eq 2). The molecular structure from X-ray crystallography confirms the increase in zwitterionic character of the amide upon ligation to the Mn atom (vide infra).

^{1}H NMR Spectra. NMR now constitutes one of the most powerful physical methods to address the ground electronic state characteristics of paramagnetic metalloporphyrins largely due to the definitive and voluminous work of La Mar, Walker, and

(27) Gouterman, M. In "The Porphyrins"; Dolphin, D., Ed.; Academic Press: New York, 1978; Vol. III, Part A, Chapter 1.
(28) Behere, D. V.; Mitra, S. *Inorg. Chem.* **1980**, *19*, 992.
(29) Rao, Ch. P.; Rao, A. M.; Rao, C. N. R. *Inorg. Chem.* **1984**, *23*, 2080.
(30) Sigel, H.; Martin, R. B. *Chem. Rev.* **1982**, *82*, 385.

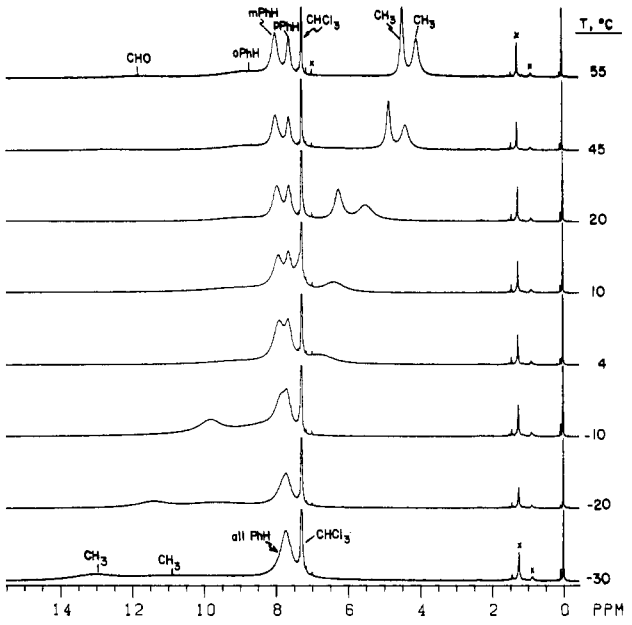

Figure 3. Representative ^1H NMR spectra for δ 0–14 (vs. Me_4Si) for **1** from −30 to +55 °C. The sample is 7.13×10^{-3} M in $CDCl_3$ ("100 atom % D", Aldrich). Peaks are assigned on the first and last spectra; × designates impurities present in the solvent.

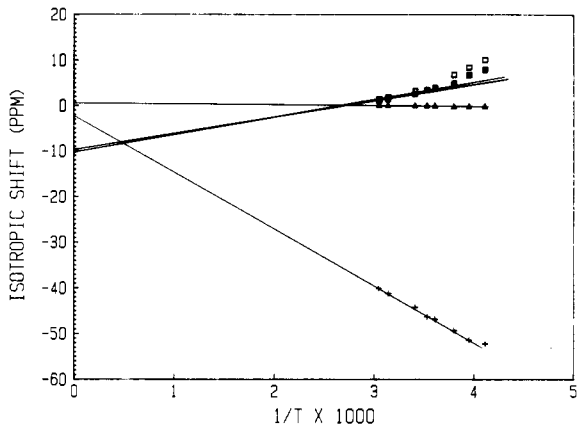

Figure 4. Isotropic shift vs. $1/T$ for **1** (7.13×10^{-3} M in $CDCl_3$; −30 to +55 °C): (+) β-pyr H; (△) meta Ph H (para Ph H with isotropic shifts almost identical with those at meta Ph H has been omitted for clarity); (□, ■) DMF CH_3.

Goff.[31-35] The line widths and relaxation behavior[34] as well as the isotropic shift behavior[35] of high-spin $S = 2$ Mn^{III} porphyrins have been reported by La Mar and Walker. The ^1H NMR spectra of low-spin $S = 1$ Mn^{III} porphyrins[22] and Mn^{II} porphyrins[36] have been studied by Hansen and Goff, and we have previously reported the ^1H NMR characteristics of monomeric and dimeric Mn^{IV} complexes[6,37] and the thermally stable diamagnetic nitrido Mn^V porphyrin complex.[11] The ^1H NMR spectral characteristics of **1** are similar to those of the high-spin Mn^{III} complexes and distinct

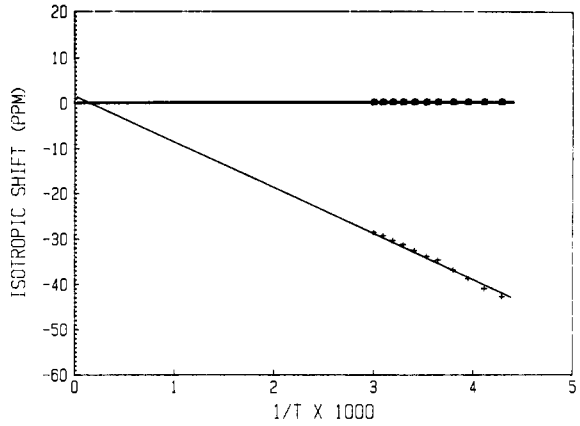

Figure 5. Isotropic shift vs. $1/T$ for $[Mn^{III}TPP(1\text{-}MeIm)_2]^+ClO_4^-$ (−40 to +60 °C). Only β-pyr H (+), 1-MeIm CH_3 (□), meta and Ph H (△) are shown for clarity. Only the isotropic shifts of β-pyrrole protons display a substantive temperature dependence.

from those of the Mn^{II}, low-spin Mn^{III}, and monomeric and dimeric Mn^{IV} and Mn^V porphyrin complexes. Figures 3–5 summarize variable-temperature ^1H NMR data for **1** and $[Mn^{III}TPP(1\text{-}MeIm)_2]^+ClO_4^-$ over temperature ranges from −40 to +60 °C. Figure 3 is a multiple overlay of the ^1H NMR spectra of **1** excluding the β-pyrrole resonances, and Figures 4 and 5 illustrate the temperature dependencies of the isotropic shifts for **1** and $[Mn^{III}TPP(1\text{-}MeIm)_2]^+ClO_4^-$, respectively. All the isotropic shifts are referenced to the diamagnetic $Zn^{II}TPP$ complex. Control experiments to check for decomposition of the complexes under the conditions of the NMR studies were executed by rerecording the ^1H NMR spectra at 25 °C after the spectra at higher temperatures had been recorded. In no case was there any detectable alteration in the chemical shifts, peak shapes, or peak widths, implying that negligible decomposition had occurred during the course of the NMR experiments. The origin of the non-zero intercepts at $T^{-1} = 0$ on the NMR Curie plots is uncertain, although such non-zero intercepts have been attributed for both low-spin Fe^{III} and high-spin Mn^{III} porphyrin complexes to a second-order Zeeman interaction.[35,38]

The isotropic shifts for all the phenyl protons on all the $[Mn^{III}TPP(L)_2]^+$ cations are very small, ruling out appreciable dipolar contributions. The β-pyrrole resonance in all the Mn^{III} cationic complexes examined at all temperatures is well upfield from Me_4Si consistent with the $d_{x^2-y^2}$ orbital being unoccupied and the d_{xz} and d_{yz} orbitals being partially occupied. The DMF methyl protons of **1** are two singlets at all temperatures with the peak-to-peak separation, $\Delta\delta$, increasing with decreasing temperature. This behavior is consistent with an increase in zwitterionic character in the DMF moieties (eq 1 and 2) and methyl protons that are diastereotopically more distinct as the temperature is lowered. All the NMR Curie law plots are quite linear for all the protons on all the cationic complexes except for the DMF methyl protons of **1** and perhaps the β-pyrrole protons. The broadness of the β-pyrrole proton resonances renders quantification of the slight degree of curvature in these plots highly uncertain. The DMF methyl proton resonances show marked curvature (Figure 4).

Curvature in plots of isotropic shift vs. T^{-1} for paramagnetic metalloporphyrins could arise for several reasons. (1) A change in spin state, a spin-state equilibrium, dynamic valence isomerism, or, less likely, more complicated temperature-dependent changes in electronic state over the measured temperature range could all produce curvature. (2) If the isotropic shifts are largely dipolar in character and the dipolar contributions arise primarily by zero-field splitting (ZFS) anisotropy, then curvature would be predicted.[32] (3) If a dynamic axial ligand exchange process with a lifetime similar to that of the NMR phenomenon is operative, then curvature would accompany the classical temperature-de-

(31) La Mar, G. N.; Horrocks, W. D.; Holm, R. H. "NMR of Paramagnetic Molecules"; Academic Press: New York, 1973.
(32) La Mar, G. N.; Walker, F. A. In "The Porphyrins"; Dolphin, D., Ed.; Academic Press: New York, 1979; Vol. IV, Part B, Chapter 2.
(33) (a) La Mar, G. N.; Eaton, G. R.; Holm, R. H.; Walker, F. A. *J. Am. Chem. Soc.* **1973**, *95*, 63–75. (b) La Mar, G. N.; Walker, F. A. *J. Am. Chem. Soc.* **1973**, *95*, 1782–1790. (c) Walker, F. A.; La Mar, G. N. *Ann. N.Y. Acad. Sci.* **1973**, *206*, 328–348. (d) Goff, H.; La Mar, G. N.; Reed, C. A. *J. Am. Chem. Soc.* **1977**, *99*, 3641–3646. (e) Goff, H.; La Mar, G. N. *J. Am. Chem. Soc.* **1977**, *99*, 6599–6606.
(34) La Mar, G. N.; Walker, F. A. *J. Am. Chem. Soc.* **1973**, *95*, 6950.
(35) La Mar, G. N.; Walker, F. A. *J. Am. Chem. Soc.* **1975**, *97*, 5103.
(36) Hansen, A. P. M.S. Thesis, University of Iowa, 1982.
(37) Camenzind, M. J. Ph.D. Thesis, University of California, Berkeley, CA, 1983. Schardt, B. C. Ph.D. Thesis, University of California, Berkeley, CA, 1984.
(38) Jesson, J. P. In ref 31, Chapter 1.

Table III. Selected Bond Lengths (Å)

Mn–O(1a)	2.217 (4)	Mn–N(1)	2.001 (4)
Mn–N(2)	2.018 (5)	N(1)–C(1)	1.400 (8)
O(1a)–C(2a)	1.273 (10)	N(2)–C(6)	1.382 (6)
N(1)–C(4)	1.393 (6)	C(1)–C(2)	1.438 (7)
N(2)–C(9)	1.388 (8)	C(2)–C(3)	1.348 (9)
C(1)–C(10)	1.392 (8)	C(4)–C(5)	1.388 (8)
C(3)–C(4)	1.425 (8)	C(5)–C(6a)	1.392 (8)
C(6)–C(7)	1.433 (9)	C(8)–C(9)	1.429 (8)
C(7)–C(8)	1.326 (9)	N(3a)–C(4a)	1.429 (9)
C(9)–C(10)	1.395 (7)	Cl–O(2)	1.396 (8)
C(2a)–N(3a)	1.318 (9)		
N(3a)–C(5a)	1.405 (13)		
Cl–O(3)	1.415 (5)		

pendent line shape changes. (4) If different thermodynamic populations of species exist at different temperatures with all the dynamic molecular processes in the fast-exchange limit even at the lowest temperature used, then curvature would also be expected.

The variable-temperature ^{1}H NMR data for **1** is most accurately rationalized by (4) above. The other possible explanations above can be systematically ruled out. Any change in spin state or the presence of a spin-state equilibrium would be evident from the magnetic susceptibility and would likely result in much greater curvature for most of the protons in the Curie plots than is observed. It is also clear from very recent work that two very strong axial ligands are required for spin pairing in Mn^{III} porphyrins to occur.[20,22] Likewise, a temperature-dependent dynamic valence isomerism, a change in the site of oxidation (reduction), metal vs. ligand (eq 3), is not operative.[39,40] The first and third isomeric

$$[Mn^{II}Por^{+\cdot}]^+ \rightleftharpoons [Mn^{III}Por]^+ \rightleftharpoons [Mn^{IV}Por^{-\cdot}]^+ \qquad (3)$$

forms of the formal Mn^{III} porphyrin in eq 3 can be ruled out. Although Goff and co-workers have characterized Mn^{III} porphyrin π-cation-radical complexes[42] and our group has demonstrated a temperature-dependent dynamic valence isomerism in the porphyrin complex $Mn^{IV}TPP(Cl)_2$,[37] the magnetic, UV–vis, and ^{1}H NMR properties of **1** rule out appreciable concentrations of either the Mn^{II} π-cation-radical or the Mn^{IV} π-anion-radical forms for this complex. Possible explanation 2 above for the curvature seen in the NMR Curie plots is very unlikely because the magnetic anisotropies and zero-field splitting parameters, D, for high-spin Mn^{III} complexes including Mn^{III} porphyrins have been measured by single-crystal magnetic susceptibility[43] and by far-infrared spectroscopy[44] and are quite small. Explanation 3 above for the curvature is ruled out by an examination of all the variable-temperature NMR data for **1** and the other cationic Mn^{III} complexes and by the fact that addition of excess DMF to **1** results in one set of DMF resonances over the entire range of temperature used in the NMR experiments. The exchange of DMF molecules on the axial positions of Mn is fast on the NMR time scale even at −40 °C.

The curvature of the DMF methyl proton plots and the linearity of the other proton plots of **1** (Figure 4) are consistent with the six-coordinate cationic form $[Mn^{III}TPP(DMF)_2]^+$ being the favored equilibrium form at low temperature and a five-coordinate form (e.g. $[Mn^{III}TPP(DMF)]^+$) plus freely diffusing DMF being the favored equilibrium forms at higher temperatures. The linearity of the plots for the TPP protons of **1** is fortuitously straight because the isotropic shift characteristics for the porphyrin protons are relatively insensitive to changes in axial ligation. The DMF protons show substantially different shifts at the high temperatures, however, because the average molecular environment for these protons is substantially different. Additional evidence for the presence of dissociated DMF in high-temperature solutions (>25 °C) of **1** is that both the chemical shifts and line widths for the protons approach those displayed by free uncomplexed DMF under the same experimental conditions.

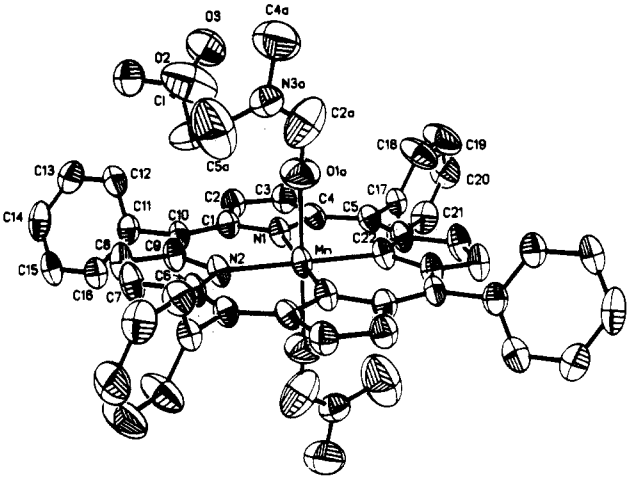

Figure 6. ORTEP[45] and atom-labeling diagram of bis(*N*,*N*-dimethylformamide)(tetraphenylporphinato)manganese(III) perchlorate (**1**) showing 50% probability ellipsoids. Hydrogen atoms are omitted for clarity. The crystallographically unique atoms are labeled.

Table IV. Selected Bond Angles (deg)

O(1a)–Mn–N(1)	89.5 (2)	O(1a)–Mn–N(2)	89.1 (2)
N(1)–Mn–N(2)	89.3 (2)	O(1a)–Mn–O(1aa)	180.0
O(1a)–Mn–N(1a)	90.5 (2)	N(1)–Mn–N(1a)	180.0
N(2)–Mn–N(1a)	90.7 (2)	Mn–O(1a)–C(2a)	173.1 (5)
O(1a)–Mn–N(2a)	90.9 (2)	Mn–N(1)–C(4)	126.5 (4)
N(2)–Mn–N(2a)	180.0	Mn–N(2)–C(6)	126.1 (4)
Mn–N(1)–C(1)	128.1 (3)	C(6)–N(2)–C(9)	106.5 (4)
C(1)–N(1)–C(4)	105.4 (4)	N(1)–C(1)–C(10)	125.5 (5)
Mn–N(2)–C(9)	127.2 (3)	C(1)–C(2)–C(3)	107.6 (5)
N(1)–C(1)–C(2)	109.2 (5)	N(1)–C(4)–C(3)	109.9 (5)
C(2)–C(1)–C(10)	125.3 (6)	C(3)–C(4)–C(5)	124.1 (4)
C(2)–C(3)–C(4)	107.9 (4)	C(4)–C(5)–C(6a)	124.3 (4)
N(1)–C(4)–C(5)	126.0 (5)	N(2)–C(6)–C(7)	108.3 (5)
C(4)–C(5)–C(17)	118.2 (5)	C(7)–C(6)–C(5a)	125.5 (4)
C(17)–C(5)–C(6a)	117.4 (5)	C(7)–C(8)–C(9)	107.6 (6)
N(2)–C(6)–C(5a)	126.2 (5)	N(2)–C(9)–C(10)	126.4 (5)
C(6)–C(7)–C(8)	108.7 (5)	C(1)–C(10)–C(9)	123.2 (6)
N(2)–C(9)–C(8)	108.9 (4)	C(2a)–N(3a)–C(4a)	116.4 (7)
C(8)–C(9)–C(10)	124.7 (6)	C(4a)–N(3a)–C(5a)	115.9 (7)
O(1a)–C(2a)–N(3a)	121.7 (8)	O(2)–Cl–O(2a)	106.9 (6)
C(2a)–N(3a)–C(5a)	127.6 (7)		
O(2)–Cl–O(3)	108.1 (4)		
O(3)–Cl–O(2a)	108.9 (3)		
O(3)–Cl–O(3a)	115.7 (5)		

X-ray Crystallography Structure of 1. The ORTEP[45] diagram and atom numbering for **1** is illustrated in Figure 6. Tables III and IV summarize selected bond lengths and bond angles in **1**, respectively.

The crystal structure is constituted by well-separated molecules of **1** that pack to define small channels. The channels are unoccupied in this solvate-free crystal structure, and the perchlorate counterion is well separated from the $Mn^{III}TPP$ cation (d_{Mn-Cl} = 7.968 Å). Complex **1** has a crystallographically imposed inversion center. The Mn atom is in the plane of the porphyrin and shows substantial distortion by tetragonal elongation as expected for a S = 2 Mn^{III} atom. The Mn^{III}–O distance of 2.217 (4) Å is the second longest distance between a DMF oxygen atom

(39) Temperature-dependent dynamic valence isomerism has been observed by Dolphin and co-workers for Ni^{III} porphyrins ($Ni^{III}OEP \rightleftharpoons Ni^{II}OEP^{+\cdot}$)[41] and by our group for Mn^{IV} porphyrins.[37]

(40) For further discussion of temperature-dependent dynamic valence isomerism see: Gagné, R. R.; Ingle, D. M. *Inorg. Chem.* **1981**, *20*, 420 and references cited therein.

(41) Johnson, E. C.; Niem, T.; Dolphin, D. *Can. J. Chem.* **1978**, *56*, 1381.

(42) (a) Goff, H. M.; Phillippi, M. A.; Boersma, A. D.; Hansen, A. P. *Adv. Chem. Ser.* **1982**, *No. 201*, 357. (b) Kelley, S. L.; Kadish, K. M. *Inorg. Chem.* **1982**, *21*, 3631.

(43) Behere, D. V.; Mitra, S. *Inorg. Chem.* **1980**, *19*, 992.

(44) Brackett, G. C.; Richards, P. L.; Caughey, W. S. *J. Chem. Phys.* **1971**, *54*, 4383.

(45) Johnson, C. K. *Oak Ridge Natl. Lab., [Rep.] ORNL (U.S.)* **1965**, *ORNL-3794*.

Table V. Comparison of Selected Bond Distances and Angles for *N,N*-Dimethylformamide in Different Molecular Environments[a]

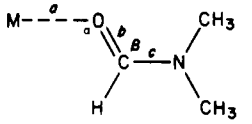

compd	*a*	*b*	*c*	*α*	*β*	ref
			Structure in This Work			
$[Mn^{III}TPP(DMF_2)]^+ClO_4^-$ (**1**)	2.217 (4)	1.273 (10)	1.318 (9)	173.1 (5)	121.7 (8)	this work
			Structures with DMF Not Coordinated			
DMF solvate in L_4Zn^{2+}·DMF	NA[c]	1.260 (9)	1.302 (9)	NA	125.6	47
BSX·DMF molecular complex	NA	1.211 (5)	1.327 (5)	NA	125.4	48
			Structures with DMF Coordinated to Main-Group Metal Ions			
LiCl·DMF·$^1/_2H_2O$	1.965 (av)[b]	1.261 (13)	1.280 (13)	131 (av)	125.4 (10)	27
$NaClO_4$·2DMF	2.37 (av)	1.227 (10)	1.318 (11)	124 (av)	125.7 (8)	27
$CaCl_2$·2DMF·$2H_2O$	2.35 (av)	1.234 (6)	1.317 (6)	128.1	124.2 (4)	27
$Mg(ClO_4)_2$·6DMF	2.05 (av)	1.24 (av)	1.308 (av)	129 (av)	124 (av)	27
Sb^VCl_5·DMF	2.048 (6)	1.300 (10)	1.287 (12)	124.49 (60)	120.15 (89)	49
			Structures with DMF Coordinated to First-Row Transition-Metal Ions			
$Cr^{III}Cl_3$(phen)DMF	1.91 (2)	1.28 (2)	1.34 (2)	128 (1)	122 (2)	52
$[Co^{II}Salen]_2O_2(DMF)_2$	2.150 (7)	1.222 (11)	1.310 (11)	121.5 (6)	126.7 (10)	53
$[Fe^{III}(DMF)_6](ClO_4)_3$	1.979 (21)	1.25 (2)	1.30 (2)	128.9 (5)	123.6 (7)	54
	1.993 (5)	1.26 (1)	1.30 (1)	124.8 (4)	124.0 (6)	
	1.997 (14)	1.27 (1)	1.30 (1)	127.6 (4)	122.5 (6)	
$Fe^{II}Pc(CO)DMF$[23]	2.07	1.18 (3)	1.34 (3)	123 (1)	123 (3)	55

[a] Distances are in angstroms and angles in degrees. [b] Average of two or more crystallographically unique distances or angles. [c] NA = not applicable.

and a first-row transition metal known (Table V). The Mn-to-N(porphyrin) distances, $d_{Mn-N(Por)}$, of 2.018 (5) and 2.001 (4) Å are typical for first-row transition-metal metalloporphyrin complexes where the σ antibonding $d_{x^2-y^2}$ orbital is unoccupied.[46] Table V summarizes key structural parameters for both free and coordinated DMF species. The DMF molecules in almost all the structures summarized in Table V, including **1**, are nearly planar, reflecting one structural consequence of the zwitterionic resonance form of an amide (eq 2). The ratio of $d_{C=O}/d_{C-N}$ in **1** is smaller than in many other main-group-metal and transition-metal complexes of DMF, reflecting again the weak bond between the $S = 2$ Mn^{III} atom and the DMF oxygen atom. The largest value for the ratio $d_{C=O}/d_{C-N}$ is seen with the strongly polarizing Sb^V atom,[49] which would be expected to form the strongest electrostatic metal–oxygen bond of the complexes studied and display the largest value of K_1 in eq 1. The porphyrin N_4 coordination environment displays some S_4 ruffling as is common in transition-metal metalloporphyrins.[46] The remaining atoms in the 24-atom core show a modest amount of out-of-plane displacement. Most of the latter displacements can be attributed to crystal-packing forces.[50]

Conclusions

In the absence of halide, pseudohalide, or strong-field ligands, Mn^{III} porphyrins exist in solution largely as six-coordinate cations, $[Mn^{III}(Por)(L)_2]^+X^-$, at 25 °C. The $[Mn^{III}TPP(L)_2]^+ClO_4^-$ complexes reported here all contain high-spin $S = 2$ Mn^{III} ions with the ground-state electronic configuration $(d_{xz}\pi, d_{yz}\pi)^2(d_{xy})^1(d_{z^2}\sigma)^1$. These complexes exchange axial ligands rapidly on the NMR time scale at temperatures down to at least −40 °C, consistent with a ground electronic state that exhibits substantial σ-antibonding character with respect to the axial ligands. Neither of the $[Mn^{III}TPP(L)_2]^+ClO_4^-$ complexes, L = DMF and 1-methylimidazole, demonstrates any change in ground electronic state over a fairly wide temperature range (−40 to +60 °C). The crystal structure of one complex, $[Mn^{III}TPP(DMF)_2]^+ClO_4^-$ (**1**), confirms a six-coordinate Mn atom with substantial tetragonal distortion manifested by elongated bonds to the axial DMF oxygen atoms. The thermodynamic coordination environment of Mn^{III} in **1** changes from six-coordinate below ca. −10 °C to five-coordinate above +10 °C.

Acknowledgment. Support of this work by the National Science Foundation (Grant No. CHE-8402994) is acknowledged. We would like to thank Don Vanderveer at the Georgia Institute of Technology for collecting the data set and for aid in the preliminary stages of the crystallographic structure determination.

Registry No. **1**, 97170-98-4; $[Mn^{III}TPP(Me\text{-}Im)]ClO_4$, 89485-48-3; $Mn^{III}TPP(ClO_4)$, 79408-54-1.

Supplementary Material Available: Crystallographic data for $[Mn^{III}TPP(DMF)_2]^+ClO_4^-$ (**1**) including listings of anisotropic temperature factors (Table SVI), hydrogen coordinates and temperature factors (Table SVII), observed and calculated structure factors (Table SVIII), nonbonded distances and torsion angles (Table SIX), and all bond distances and angles (Table SX) and a stereoview of the crystal-packing diagram (27 pages). Ordering information is given on any current masthead page.

(46) Scheidt, W. R. In "The Porphyrins"; Dolphin, D., Ed.; Academic Press: New York, 1978; Vol. III, Part A, Chapter 10, and references cited therein.
(47) Read, R. J.; James, M. N. G. *J. Am. Chem. Soc.* **1981**, *103*, 6947.
(48) Cobbledick, R. E.; Small, R. W. H. *Acta Crystallogr., Sect. B: Struct. Crystallogr. Cryst. Chem.* **1973**, *B29*, 1659.
(49) Brun, L.; Bränden, C. I. *Acta Crystallogr.* **1966**, *20*, 749.
(50) Evidence from several metalloporphyrin crystal structures establishes conclusively that crystal-packing forces can play a major role in deviations from planarity of the 24-atom porphyrin ring in metalloporphyrin crystal structures. The most compelling evidence comes from the $Ni^{II}OEP$ complex, whose structure has been determined in two different crystalline forms that vary greatly in the planarity of the porphyrin ring.[51] Two different X-ray crystallographic structure determinations have been carried out on nitrido Mn^V tetraarylporphyrins that also implicate forces other than those intrinsic to the molecule itself largely dictate the degree of deformity observed in the porphyrin ring.
(51) Cullen, D. L.; Meyer, E. F., Jr. *J. Am. Chem. Soc.* **1974**, *96*, 2095.
(52) Broomhead, J. A.; Evans, J.; Gromley, W. D.; Sterns, M. *J. Chem. Soc., Dalton Trans.* **1977**, 173.
(53) Calligaris, M.; Nardin, G.; Randaccio, L.; Ripamonti, A. *J. Chem. Soc. A* **1970**, 1069.
(54) Holt, E. M.; Alcock, N. W.; Summer, R. H.; Asplund, R. O. *Cryst. Struct. Commun.* **1979**, *8*, 255.
(55) Calderazzo, F.; Pampaloni, G.; Vitali, D.; Pelizzi, G.; Collamati, I.; Frediani, S.; Serra, A. M. *J. Organomet. Chem.* **1980**, *191*, 217.